Eur. Phys. J. B **26**, 431–434 (2002)
DOI: 10.1140/epjb/e20020110

THE EUROPEAN PHYSICAL JOURNAL B
EDP Sciences

Magnetic-roughness-induced magnetostatic interactions in magnetic tunnel junctions

C. Tiusan[1], M. Hehn[1,a], and K. Ounadjela[2]

[1] Laboratoire de Physique des Matériaux, BP 239, 54506 Vandœuvre-lès-Nancy, France
[2] Institut de Physique et de Chimie des Matériaux de Strasbourg[b], 23 rue du Loess, 67037 Strasbourg Cedex, France

Received 7 December 2001

Abstract. Magnetostatic ferromagnetic coupling in magnetic tunnel junctions was selectively analyzed. We have shown that in samples involving polycrystalline magnetic films, beyond the orange-peel coupling, an important class of interaction is related to the dispersion fields associated to magnetic inhomogeneities. These magnetization fluctuations were described in terms of magnetic roughness arising from the local anisotropy fluctuations. Therefore, using roughness data extracted from atomic/ magnetic force microscopy analysis, the amplitude and the variation with distance of the magnetostatic interactions were selectively quantified.

PACS. 75.60.-d Domain effects, magnetization curves, and hysteresis – 73.43.Jn Tunneling – 73.40.Rw Metal-insulator-metal structures

The increasing implication of magnetic tunnel junctions (MTJs) for spin electronic devices requires the understanding and the control of the magnetic properties of their ferromagnetic (FM) electrodes. Beyond aspects concerning the magnetism of ferromagnetic metal/insulator interfaces in MTJs, an important parameter is the coupling between the two electrodes of the MTJ. These interactions between the magnetically hard (reference) and the soft (detection) layer of the MTJ are of particular importance as they influence the reversal characteristics of the FM layers, and thus, the magnetoresistive response of the tunnel device.

Several mechanisms can be implicated in the magnetic coupling between two FM films separated by a thin insulating layer. However, when assuming a continuous and pinhole-free insulating layer, the direct FM coupling associated to discontinuity of the insulator can be excluded. Moreover, when the voltage dependent coupling induced by the tunnelling of spin polarized electrons [1] is negligible, the most important class of interactions is magnetostatic. In this last category, two main contributions have been identified. The first one is the antiferromagnetic coupling related to the lateral flux closure of the stray fields between the magnetic layers of the MTJ. It becomes significant when reducing the lateral size of the MTJ FM electrodes and increasing their aspect ratio [2]. The second contribution is related to stray fields induced by magnetic charge accumulations in the junction's ferromagnetic layers and is usually associated to the roughness of the interfaces, referred as the orange-peel effect [3,4].

The contribution of *intrinsic* charge accumulations linked to the presence of magnetization inhomogeneities like domain walls has recently been addressed [5] and demagnetization of the hard magnetic layer of a tunnel junction by sweeping domain walls in the soft magnetic layer has been shown. However, in polycrystalline magnetic hard materials, a reciprocal situation can exist: the local anisotropy fluctuations in the hard magnetic layer act as an additional source of charge accumulations created by magnetization fluctuations. Those fluctuations, described in terms of *magnetic roughness*, are responsible for coupling effects similar to the orange-peel. Moreover, the range of these interactions can be significantly larger than the one of the orange-peel. The main point of our paper is that the effect of the magnetic roughness – related coupling has to be always considered when discussing ferromagnetic coupling between active polycrystalline magnetic layers in multilayer systems, beyond the commonly reported orange-peel.

Magnetic tunnel junctions, with lateral size superior to 10 μm to reduce the dipolar antiferromagnetic coupling intensity, are elaborated in a complex stack [6]. First, a Cr(1.6 nm)/Fe(6 nm)/Cu(30 nm) buffer layer is grown on a Si(111) wafer. In the following, the 6 nm thick Fe layer incorporated in this buffer tri-layer is referenced as the Fe layer. On the top of the buffer, a magnetically hard subsystem constituted by an antiferromagnetically coupled trilayer CoFe(1.8 nm)/Ru(0.8 nm)/CoFe(3 nm) is stacked. This hard subsystem is separated by a 1–2 nm thick Al

[a] e-mail: hehn@lpm.u-nancy.fr
[b] UMR CNRS 7504

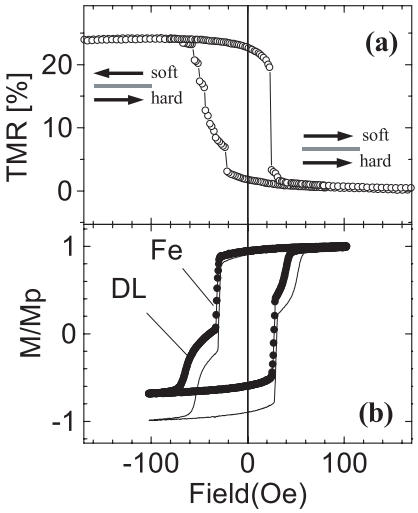

Fig. 1. (a) Minor magnetoresistance loop measured on a CoFe/Ru/CoFe/AlOx/CoFe/Fe MTJ. Arrows illustrate the magnetizations of the DL and of the hard subsystem layer in contact with the tunnel barrier; (b) Minor magnetization loop for a continuous film MTJ stack measured in two distinct situations: the hard CoFe/Ru/CoFe layer is in a remanent (-•-) or a demagnetized (—) state.

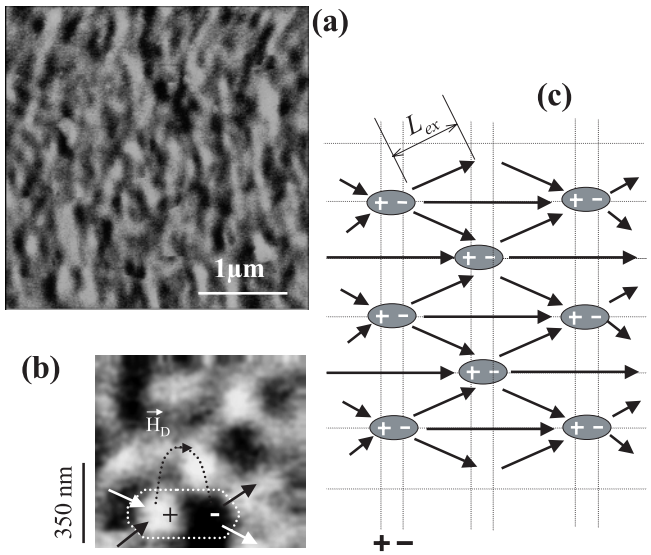

Fig. 2. (a) MFM image of the remanent state of the MTJ hard CoFe/Ru/CoFe subsystem. Alternating black and white stripes are directly associated to the magnetic dipoles, clearly illustrated in Figure (b) (zoom of Fig. (a)). (c) Sketch in two dimensions, for the magnetization configuration, used to explain the MFM contrast of Figure (a). The periodic array of dipoles gives rise to parallel lines of successive positive and negative local charge accumulations, responsible of repulsive respectively attractive interactions with the MFM tip. The dipole associated stray field $\boldsymbol{H}_D$, going from the positive to the negative charges is illustrated in (b).

oxide barrier from a CoFe(1 nm)/Fe(6 nm) magnetically soft subsystem protected by a Cu(5 nm)/Cr(3 nm) bilayer. In the following, the CoFe(1 nm)/Fe(6 nm) bilayer is referenced as detection layer or DL. Then, the hard CoFe/Ru/CoFe subsystem is separated from the Fe layer with a 30 nm thick Cu layer, and from the DL with a 1–2 nm thick Al oxide layer.

Analysis of cross-section transmission electron microscopy images as well as tunnel barrier mapping measurements [7] revealed a good quality and continuous insulating layer. Therefore the direct FM coupling is automatically excluded. However, tunnel magneto-transport measurements show a net ferromagnetic coupling between the hard CoFe/Ru/CoFe subsystem and the DL as illustrated by Figure 1a. In this measurement, only the switching of the DL is observed since spin polarised tunnelling is sensitive to the magnetization alignement of the layers in contact with the barrier. The sharp reversal corresponds to the DL switching from the antiparallel to the parallel configuration with respect to the hard layer net moment. This reversal is completed at a field around 40 Oe. When the DL switches from the parallel to the antiparallel configuration, the reversal occurs in successive steps, sign of wall blocking phenomena, and is completed only at fields around 70 Oe leading to the appearance of a field bias offset. This set of measurements has been performed for bias voltage applied to the junction ranging from 5 to 100 mV. No variation of the coupling with dc bias was detected. Moreover, the intensity of the coupling strength was found to increase when decreasing the barrier thickness or increasing the net magnetic moments of the junction's ferromagnetic subsystems. Therefore we conclude that the FM coupling in our system is purely magnetostatic.

More insight in the magnetostatic coupling origin in our MTJs is given by the study of the magnetization reversal of the Fe layer in the buffer stack measured on conventional magnetization loops. Therefore, in Figure 1b, the reversals of both buffer Fe and DL layers are observed. The buffer Fe layer is separated from the hard subsystem by a 30 nm thick Cu layer. Therefore, for this layer typical orange-peel magnetostatic coupling with the hard subsystem should be insignificant and a direct RKKY coupling across this thick Cu layer is also excluded. However, a field offset of ∼5 Oe can be measured on the curve obtained with the hard subsystem in a magnetic remanent configuration (Fig. 1b, $-\bullet-$). This field offset disappears as soon as the hard subsystem is in a demagnetized state (Fig. 1b, continuous line).

It appears then that one of the origins of the FM coupling in our MTJ stack is dependent on the microscopic magnetization state of the hard CoFe/Ru/CoFe subsystem. We attribute this coupling to dispersion fields associated to magnetic inhomogeneities *i.e.* small angular fluctuations of magnetization in the hard magnetic system [8]. Their associated stray fields influence the local field experienced by a 'neighbor' magnetic layer having a direct impact on the layer's magnetization reversal. In order to quantify these interactions a model based on the concept of 'magnetic roughness' (similar to the orange-peel Neel model) was developed, as illustrated in Figure 2. Figure 2a shows a magnetic force microscopy (MFM)

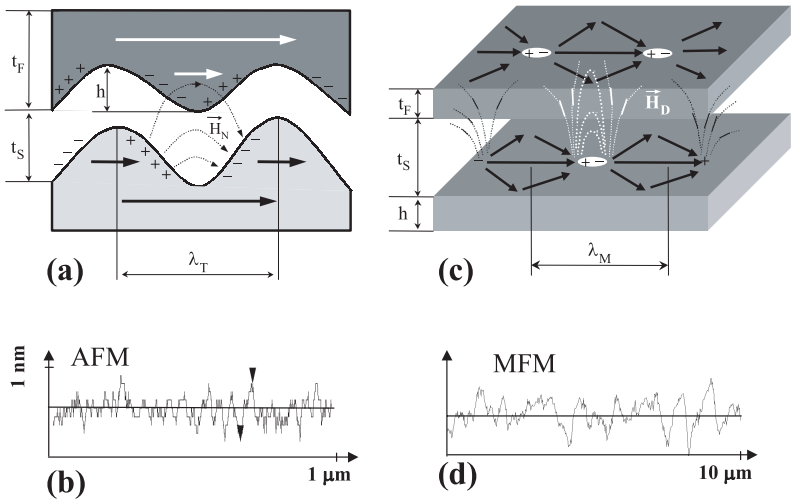

Fig. 3. Model used to quantify the coupling field associated to a periodic arrangement of magnetic dipoles. The origin of these dipoles is either the correlated topographical roughness (a) or the magnetic roughness (c). The full-line arrows depict the in-plane magnetization configuration while the dotted-lines depict the associated stray fields $\boldsymbol{H}_N$ and $\boldsymbol{H}_D$. Conventionally, the fields go from positive to negative charges. The characteristic lengths, illustrated on these pictures, can be extracted from cross sections taken on AFM (b) respectively MFM (d) pictures.

measurement performed in the remanent state of the hard subsystem. The black (resp. white) contrasts correspond to repulsive (resp. attractive) interactions of the tip with the stray fields from the local charge accumulations derived from the small angular fluctations of magnetization inside the polycristalline layer. The presence of dipoles is clearly confirmed in Figure 2b and in the remnant state, all the dipoles are oriented in the same direction leading to the appearance of a sequence of white/dark stripes (Fig. 2a). We sketched this magnetization configuration in Figure 2c. Since the length of the dipoles is less or equal to the length of the non horizontal arrows (equal to the exchange length, L_{ex}), the length of the dipoles and the distance between them are not equivalent along the applied field direction (horizontal lines). The stray fields associated to all these dipoles add up and the resultant field is not zero and oriented along the hard subsystem's net moment. It acts as a positive biasing field for the DL and Fe magnetization reversal, and is equivalent to a FM coupling which is observed in our junctions. We have validated our model by demagnetizing the hard subsystem. In this case, the magnetization of each dipole is randomly oriented, resulting in a zero global stray field and no FM coupling of the buffer Fe layer and the hard subsystem (Fig. 1b, curve (—)).

In conclusion, either topographic or remanent magnetic roughnesses generate equivalent periodic arrays of magnetic dipoles. The stray field associated to these dipoles can be selectively quantified using data extracted from AFM/MFM measurements. To estimate the coupling field H, associated to each type of roughness, we used the equation derivated previously for the orange-peel coupling [3].

$$H = \frac{\pi^2}{\sqrt{2}} \left(\frac{h^2}{\lambda t_F} \right) M_s \exp\left(-2\pi\sqrt{2} t_s / \lambda \right) \cdot \qquad (1)$$

Indeed, our assumption steams on a correlated roughness configuration, for both topographical and magnetical roughness patterns. This favors a net ferromagnetic coupling. Alternatively, we mention that for the anticorrelated situation a biquadratic coupling would be favored, as shown in previous theoretical works [4]. The anticorellated configuration is not addressed here, as long as the net coupling measured in our samples was long-range ferromagnetic-like. The assumption of correlated roughness, as illustrated in Figures 3a, c, is reasonable for both topographical and magnetical roughness. Indeed, topologically, the correlation of the interfacial roughness in our samples has been validated by cross-section transmission electron microscopy analysis, as shown in our previous work [8]. Moreover, as illustrated by Figure 3c, the magnetic roughness is also correlated by the 'mirroring' of the dipole patterns in the hard (bottom) and the soft (top) layers. Indeed, the dipolar fields associated to the magnetic dipoles in the hard layer modulate the magnetization configuration in the soft layer. Therefore, correlated image dipoles are generated in the soft layer (Fig. 3c, similarly to the corresponding correlated roughness configuration, illustrated in Fig. 3a).

The significance of each term is illustrated in Figure 3: t_F and t_s represent the thickness of the soft respectively insulating spacer layer; λ_T, λ_M the period of the topographic respectively magnetic roughness; h the amplitude of roughness fluctuations. For the topographic roughness, we used for h the peak to peak value evaluated from the cross section AFM measurement. In the case of the magnetic roughness, h was correlated with the thickness of the hard subsystem, where the magnetic fluctuations occur. M_s is the unit volume saturation magnetization for the hard subsystem magnetic material.

The cross section in the AFM (Fig. 3b) and MFM (Fig. 3d) images illustrate that roughly $\lambda_M > 10\lambda_T$.

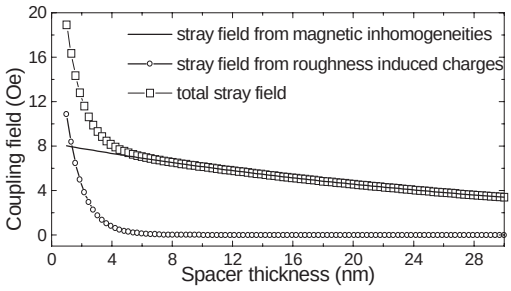

Fig. 4. Calculated stray fields originating from topographic and magnetic roughnesses as a function of distance to the hard CoFe/Ru/CoFe subsystem.

Therefore, as calculated using the equation (1) and illustrated in Figure 4, the stray field originating from the roughness induced charges vanishes exponentially at short distance (4–6 nm) while the stray field associated to magnetic inhomogeneities has a much longer range. Indeed, this stray field remains significant at a distance of 30 nm ($\sim$4 Oe) and in good agreement with the offset measured for the Fe buffer layer ($\sim$5 Oe from Fig. 1b). Therefore, at long distance, the main magnetostatic interactions are related to the magnetic roughness associated stray fields while at short distance, the layers probe the contributions of both orange-peel and magnetic roughness stray fields simultaneously. The long distance magnetic roughness associated stray fields could however not be experimentally varied. Indeed, the reduction of the Cu layer increases the RKKY interaction between the buffer Fe layer and the hard subsystem while an increase of the Cu layers increases the buffer roughness and so changes the magnetic properties of the hard subsystem. In the case of our MTJ, we estimate for the DL spaced of about 1 nm from the hard subsystem, an average orange-peel coupling of about 11 Oe while the magnetic roughness induced coupling was estimated to about 8 Oe. Therefore, the estimated resulting coupling field acting on the DL ($\sim$ 20 Oe) is in good agreement with the measured offset field in the magneto-transport curves (Fig. 1).

In conclusion, the reduction of magnetostatic coupling interactions involved in MTJs covers two aspects. First, the coupling associated to topographic roughness is a short range coupling. It can be significantly reduced by decreasing the interfacial roughness or increasing the insulating barrier thickness. Up to now, it was the most common solution invoked to reduce the electrode ferromagnetic coupling. However in polycrystalline materials often used as hard magnetic electrodes, the spatial distribution of local anisotropies creates magnetic roughness which gives rise to a long range magnetostatic coupling. This coupling can be reduced using growth conditions of the magnetic layers which stabilize an uniaxial magnetic anisotropy. This innovative solution paves the way to further reduce the electrode coupling when interfacial roughness or insulating barrier thickness are pushed to their limits.

This work was supported by the European Framework IV Materials Technology Programme, the Nanomem Programme (IST-1999-13741). The authors thank C. Meny, V. Da Costa, G. Wurtz and G. Ehret for help with the experiments. M.H. acknowledges fruitful discussions with F. Montaigne and A. Schuhl.

References

1. J.C. Slonczewski, Phys. Rev. B **39**, 6995 (1989).
2. A. Anguelouch, B. Shrang, G. Xiao, Y. Lu, P. Trouilloud, W.J. Gallagher, S.S.P. Parkin, Appl. Phys. Lett. **76**, 622 (2000).
3. L. Néel, C.R. Acad. Sci. **255**, 1676 (1962).
4. S. Demokritov, E. Tsymbal, P. Grünberg, W. Zinn, I.K. Schuller, Phys. Rev. B **49**, 720 (1994).
5. L. Thomas, M.G. Samant, S.S.P. Parkin, Phys. Rev. Lett. **84**, 1816 (2000).
6. C. Tiusan, M. Hehn, K. Ounadjela, Y. Henry, J. Hommet, C. Meny, H.A.M. van den Berg, L. Baer, R. Kinder, J. Appl. Phys. **8**, 5276 (1999).
7. V. da Costa, C. Tiusan, T. Dimopoulos, K. Ounadjela, Phys. Rev. Lett. **85**, 876 (2000).
8. C. Tiusan, T. Dimopoulos, K. Ounadjela, M. Hehn, H.A.M. van den Berg, Y. Henry, V. Da Costa, Phys. Rev. B **61**, 580 (2000).